# APPLICATION OF A FULL POTENTIAL METHOD TO AGARD STANDARD AIRFOILS

WOODROW WHITLOW, JR.
UNSTEADY AERODYNAMICS BRANCH
NASA LANGLEY RESEARCH CENTER

## OUTLINE

An outline of the presentation is shown here. First, the motivation for performing this research is discussed. Next, the formulation of an isentropic full potential method is presented, followed by a nonisentropic method. Since the methods that are presented use body-fitted grids, methods for modeling the motions of dynamic grids are presented. Computed results for the NACA 0012 and NLR 7301 airfoils are shown. Summary statements about this effort are presented, and some conclusions are made.

O MOTIVATION

O ISENTROPIC FULL POTENTIAL

O NONISENTROPIC FULL POTENTIAL

O DYNAMIC GRIDS

O RESULTS (NACA 0012, NLR 7301)

O SUMMARY

O CONCLUSIONS

## MOTIVATION

One of the most important uses of methods that calculate unsteady aerodynamic loads is to predict and analyze the aeroelastic responses of flight vehicles. Currently, methods based on transonic small disturbance (TSD) potential aerodynamics are the the primary tools for aeroelastic analysis. Theoretically, TSD methods are limited to thin bodies undergoing small amplitude motions. Full potential (FP) methods do not have these limitations, but flow solutions obtained using isentropic potential theory--TSD or FP--can be highly inaccurate and even multivalued. This is because isentropic potential methods do not model the effects of entropy that is produced when shock waves are in the flow field. Thus, the goal of this effort is to develop an unsteady full potential method that models the effects of shock-generated entropy.

O TRANSONIC SMALL DISTURBANCE THEORY IS THE PRIMARY AERODYNAMIC TOOL FOR ANALYZING TRANSONIC AEROELASTIC PHENOMENA

O TSD LIMITED TO THIN BODIES UNDERGOING SMALL AMPLITUDE MOTIONS

O SOLUTIONS FROM ISENTROPIC POTENTIAL THEORY CAN BE HIGHLY INACCURATE AND MULTIVALUED

O GOAL OF THE PRESENT EFFORT IS TO DEVELOP AN UNSTEADY FULL POTENTIAL METHOD THAT MODELS NONISENTROPIC EFFECTS

# ISENTROPIC FULL POTENTIAL
## (GENERALIZED COORDINATES)

Shown here is the formulation of the isentropic full potential method in generalized coordinates. The first equation is the continuity equation in strong conservation form, where $\tau$ is computational time, and $\xi$ and $\zeta$ are the computational coordinate directions around and normal to the airfoil, respectively. Density $\rho$ is given by the expression in the second equation, where $\gamma$ is the ratio of specific heats, M is free stream Mach number, $\phi$ is the velocity potential, and the nondimensional physical time is denoted by t. The variables U and W are the contravariant velocities in the $\xi$ and $\zeta$ directions, respectively. The metrics of the body-fitted grid are $A_1$, $A_2$, and $A_3$. The Jacobian of the coordinate transformation is given by J, and $\hat{\rho}$ is the density divided by the Jacobian. The density, biased to introduce artificial viscosity and capture shock waves, is denoted by $\tilde{\rho}$.

$$\hat{\rho}_\tau + \left(\frac{\tilde{\rho}U}{J}\right)_\xi + (\hat{\rho}W)_\zeta = 0$$

$$\rho = \left\{1 + \frac{\gamma-1}{2}[M^2 - 2\phi_\tau - (U+\xi_t)\phi_\xi - (W+\zeta_t)\phi_\zeta]\right\}^{\frac{1}{\gamma-1}}$$

$$U = \xi_t + A_1\phi_\xi + A_2\phi_\zeta \qquad\qquad W = \zeta_t + A_2\phi_\xi + A_3\phi_\zeta$$

$$J = \xi_x\zeta_z - \xi_z\zeta_x$$

$$\hat{\rho} = \frac{\rho}{J} \qquad\qquad\qquad \tilde{\rho} = \text{biased density}$$

160

# ISENTROPIC FULL POTENTIAL
## (FACTORIZATION)

The isentropic full potential formulation is linearized and factored as shown in this figure. Here, $L_\xi$ and $L_\zeta$ represent differential operators in the $\xi$ and $\zeta$ directions. The right side of the factored equation is the discretized form of the continuity equation plus some other terms not shown. The subscripts i and j represent grid points in the $\xi$ and $\zeta$ directions, respectively, and the superscripts n and n-1 represent computational time levels. Solutions for $\phi$ are advanced in time by adding the potential from the previous time step $\phi^n$ to the correction $\Delta\phi$.

$$L_\xi L_\zeta \Delta\phi = \frac{h^2}{\beta^n}[(\frac{\hat{\rho}^n - \hat{\rho}^{n-1}}{h})_{i,j} + (\frac{\tilde{\rho U}}{J})^n_{i+1/2,j} -$$

$$(\frac{\tilde{\rho U}}{J})^n_{i-1/2,j} + (\hat{\rho W})^n_{i,j+1/2} - (\hat{\rho W})^n_{i,j-1/2}] + ...$$

$$\Delta\phi = \phi^{n+1} - \phi^n$$

$$h = \Delta\tau$$

$$\beta = \frac{\rho^{2-\gamma}}{J}$$

# FLUX BIASED DIFFERENCING

The flow equations are discretized spatially using flux biased differencing. Artificial viscosity, necessary to capture shock waves, is introduced into the difference equations by defining the biased density $\rho$ as shown in the figure. The $(\rho q)^-$ term is the difference between the actual flux $\rho q$ and the sonic flux $\rho^*q^*$ in supersonic regions and is zero in subsonic regions. Expressions for the total speed q, sonic speed q*, and sonic density $\rho^*$ are shown in the figure.

$$\tilde{\rho} = \frac{1}{q}[\rho q - \Delta\xi(\rho q)_{\xi}^-]$$

$$(\rho q)^- = \rho q - \rho^*q^* \qquad\qquad q > q^*$$

$$\qquad\qquad 0 \qquad\qquad\qquad q \leq q^*$$

$$q^2 = A_1\phi_{\xi}^2 + 2A_2\phi_{\xi}\phi_{\zeta} + A_3\phi_{\zeta}^2$$

$$q^{*2} = \frac{2}{\gamma+1}[1 + \frac{\gamma-1}{2}(M^2 - 2\phi_{\tau} - 2\xi_t\phi_{\xi} - 2\zeta_t\phi_{\zeta})]$$

$$\rho^* = (q^{*2})^{\frac{1}{\gamma-1}}$$

## CHARACTERISTICS OF FLUX BIASED DIFFERENCING

Flux biased differencing (a) accurately tracks sonic conditions and automatically specifies the correct amount of artificial viscosity, (b) produces no velocity overshoots at shock waves, allowing for larger time steps for unsteady calculations, (c) produces well defined, monotone shock profiles with a maximum two point transition between the upstream and downstream states, and (d) dissipates expansion shocks, ruling out solutions with such nonphysical characteristics.

O AUTOMATICALLY SPECIFIES CORRECT AMOUNT OF ARTIFICIAL VISCOSITY

O ALLOWS FOR LARGER TIME STEPS

O PRODUCES TWO POINT SHOCK WAVES

O DISSIPATES EXPANSION SHOCKS

# NONISENTROPIC DENSITY

To model the jump in entropy across shock waves, the density downstream of shock waves is modified to $\rho_i e^{-\Delta s/R}$. The entropy jump is a function of the normal Mach number upstream of the shock wave $M_n$. The isentropic density is given by the expression in the figure and is the same as that shown in the formulation of the isentropic potential method. When the expression for the nonisentropic density is inserted into the continuity equation, the equation at the bottom of the figure is obtained. Except across shock waves and wakes, the last part of that equation vanishes. Thus, except at those locations, it is necessary only to solve the classical full potential equation.

$$\rho = \rho_i e^{\frac{-\Delta s}{R}} \qquad \Delta s = f(M_n^2)$$

$$\rho_i = (1 + (\frac{\gamma-1}{2})[M^2 - 2\phi_\tau - (U+\xi_t)\phi_\xi - (W+\zeta_t)\phi_\zeta])^{\frac{1}{\gamma-1}}$$

$$e^{\frac{-\Delta s}{R}}[\hat{\rho}_{i\tau} + (\frac{\tilde{\rho_i}U}{J})_\xi + (\hat{\rho_i}W)_\zeta] + \rho_i e^{\frac{-\Delta s}{R}}\frac{D}{Dt}(\frac{\Delta s}{R}) = 0$$

# NONISENTROPIC FULL POTENTIAL
## (FACTORIZATION)

When nonisentropic effects are modeled, the factored equation becomes as shown at the top of the figure. The nonisentropic biased density for U > 0 is given by the expression at the bottom of the figure.

$$L_\xi L_\zeta \Delta\phi = \frac{h^2}{\beta^n}\left[\frac{(\hat{\rho_i}e^{\frac{-\Delta s}{R}})^n_{i,j} - (\hat{\rho_i}e^{\frac{-\Delta s}{R}})^{n-1}_{i,j}}{h} + (\frac{\widetilde{\rho U}}{J})^n_{i+1/2,j} - (\frac{\widetilde{\rho U}}{J})^n_{i-1/2,j}\right.$$

$$\left. + (\hat{\rho_i}e^{\frac{-\Delta s}{R}}W)^n_{i,j+1/2} - (\hat{\rho_i}e^{\frac{-\Delta s}{R}}W)^n_{i,j-1/2}\right] + \ldots$$
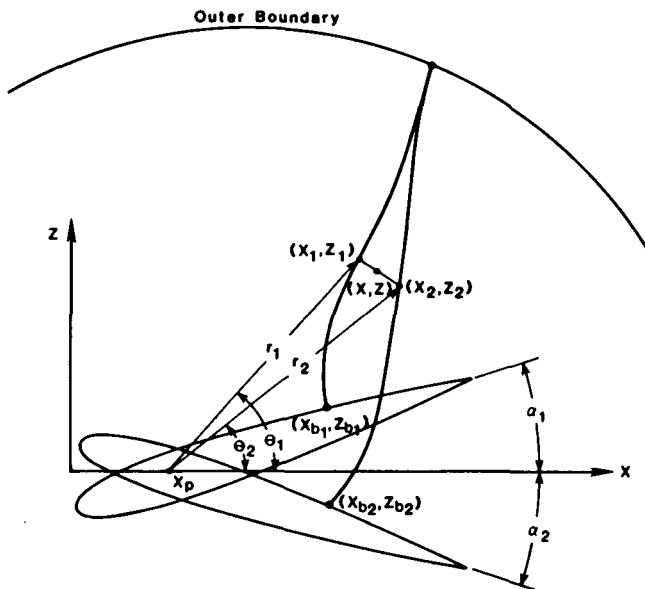
$$\widetilde{\rho}_{i+1/2,j} = (\rho_i e^{\frac{-\Delta s}{R}})_{i+1/2,j} + \frac{1}{q_{i+1/2,j}}(\rho_i q - \rho^* q^*)_{i-1/2,j}$$

# DYNAMIC GRIDS

To apply the airfoil surface boundary conditions at the instantaneous surface position requires a new grid at each time step. For this work, the body-fitted grids were generated using an elliptic method. Using this method, the resources required to generate the grids can be more than those necessary to do the aerodynamic calculations. Thus, an efficient grid interpolation method is used to generate the required grids. To simulate harmonic motions, the elliptic method is used to calculate grids at the extreme airfoil positions, and the grids for all other airfoil positions are generated using linear interpolation. Interior grid points are redistributed at each time step, while points on the outer boundary remain fixed.

The figure shows grid interpolation for an airfoil pitching about a point $x_p$. A polar coordinate system centered at $x_p$ is used. Using the subscripts 1 and 2 to denote the minimum and maximum pitch angles, the position of each grid point at any time $\tau$ is given by the expressions for $r(\tau)$ and $\theta(\tau)$. The interpolated grid points are then obtained from the expressions for $x(\tau)$ and $z(\tau)$ given in the figure.

O ASSUME LINEAR VARIATION BETWEEN EXTREME POSITIONS

O OUTER BOUNDARY FIXED



$$r(\tau) = r_1 + \frac{\alpha(\tau) - \alpha_1}{\alpha_2 - \alpha_1}(r_2 - r_1)$$

$$\theta(\tau) = \theta_1 + \frac{\alpha(\tau) - \alpha_1}{\alpha_2 - \alpha_1}(\theta_2 - \theta_1)$$

$$x(\tau) = r(\tau)\cos\theta(\tau) + x_p$$

$$z(\tau) = r(\tau)\sin\theta(\tau)$$

166

# NACA 0012
## STEADY FLOW SOLUTIONS
## M = 0.84, α = 0°

This figure shows steady pressures that are calculated on the NACA 0012 airfoil using the isentropic and nonisentropic full potential (FP) methods and an Euler method for M = 0.84, α = 0°. For this airfoil, the flow conditions are in the region where multiple solutions are known to occur. The isentropic FP result is asymmetric with negative lift. The Euler solution is symmetric with zero lift. The nonisentropic FP calculation yields a symmetric, nonlifting pressure distribution that shows good agreement with the Euler pressures. Thus, the nonisentropic FP method eliminates the phenomenon of multiple flow solutions.
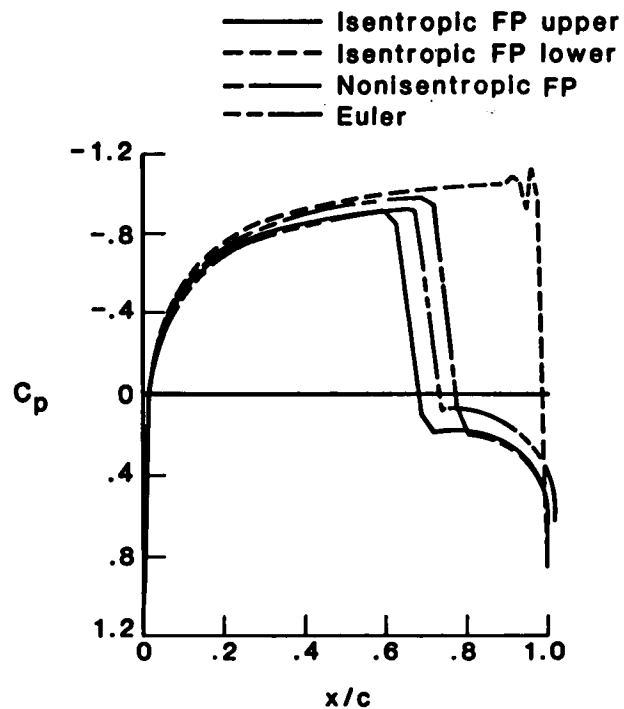
## NACA 0012
## ISENTROPIC COMPUTATIONS
## M = 0.755, α = 0.016° + 2.51°SIN(Kτ), K = 0.814

This figure shows comparisons of calculated isentropic transonic small disturbance and full potential (FP) unsteady pressures with experimental data. Generally, the FP pressures are in good agreement with experiment, but the shock wave is too strong and located too far aft on the airfoil.
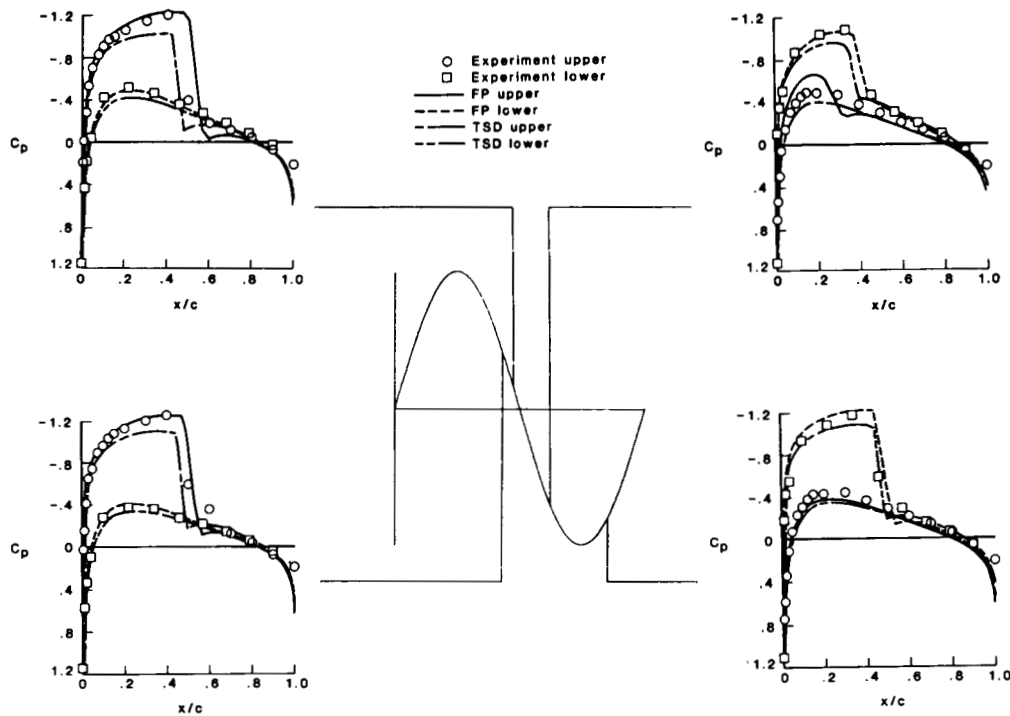
# NACA 0012
## NONISENTROPIC COMPUTATIONS
## M = 0.755, α = 0.016° + 2.51°SIN(Kτ), K = 0.0814

This figure shows comparisons of isentropic and nonisentropic full potential (FP) pressures with experimental data. Generally, the effects of modeling the shock-generated entropy are to weaken the shock wave and move it forward on the airfoil. As a result, the nonisentropic FP calculations show improved agreement with the experimental data.
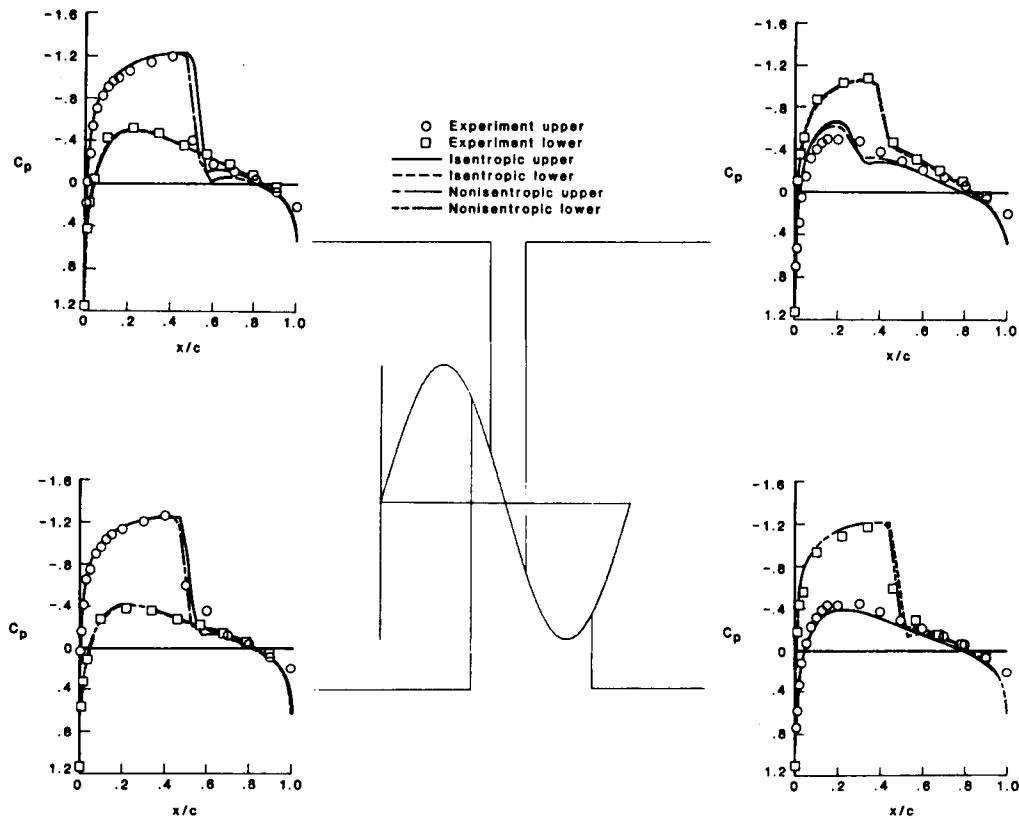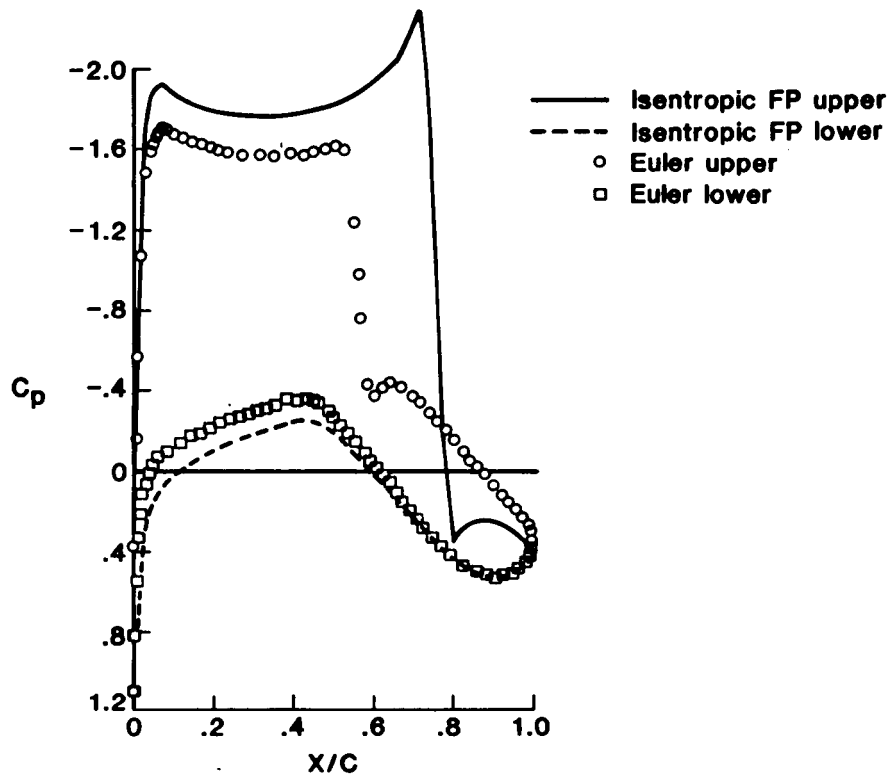
# NLR 7301
## STEADY STATE PRESSURES
### M = 0.721, α = -0.19°

Shown in this figure are comparisons of the full potential (FP) pressures with Euler calculations and experimental data for the NLR 7301 airfoil at M = 0.721, α = -0.19°. For this case, the effects of shock-generated entropy are small, and the two FP solutions are nearly identical. Thus, the isentropic and nonisentropic FP calculations are shown as one line, designated "FP". Results obtained using the potential methods show very good agreement with experimental data and with the Euler calculations. The shock location is slightly upstream of the experimental location and slightly downstream of the location predicted by the Euler method.
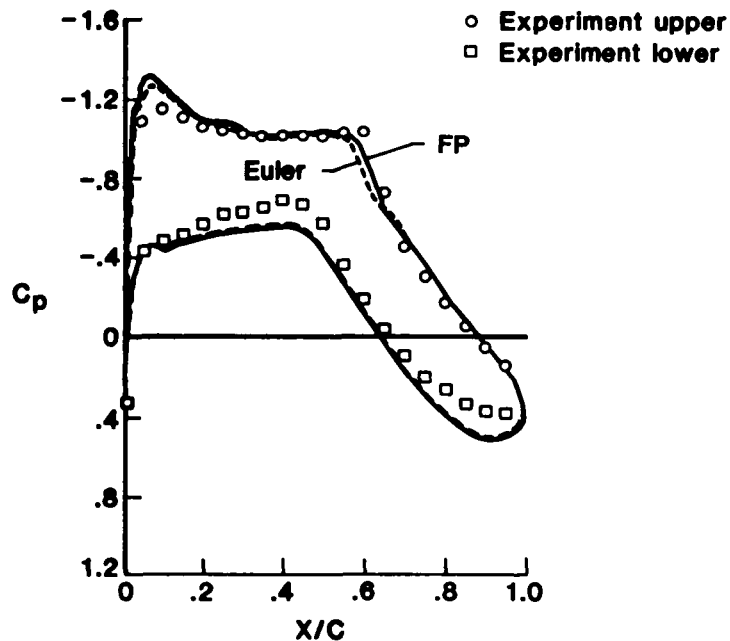
# NLR 7301
## STEADY STATE PRESSURES
### M = 0.7, α = 2°

This figure shows a comparison of isentropic potential and Euler pressures on the NLR 7301 airfoil for M = 0.7, α = 2°. The shock wave calculated with the isentropic method is too strong and located too far aft on the airfoil, suggesting that this case is outside the range of validity of the method.

# NLR 7301
## STEADY STATE PRESSURES
## M = 0.7, α = 2°

Modeling the nonisentropic effects brings the potential flow solution into good agreement with the Euler results. The shock waves differ in location by only 3 percent chord and have nearly the same strength. In addition, the agreement of pressures on the lower surface is excellent.

Nonisentropic FP upper
Nonisentropic FP lower
o  Euler upper
□  Euler lower
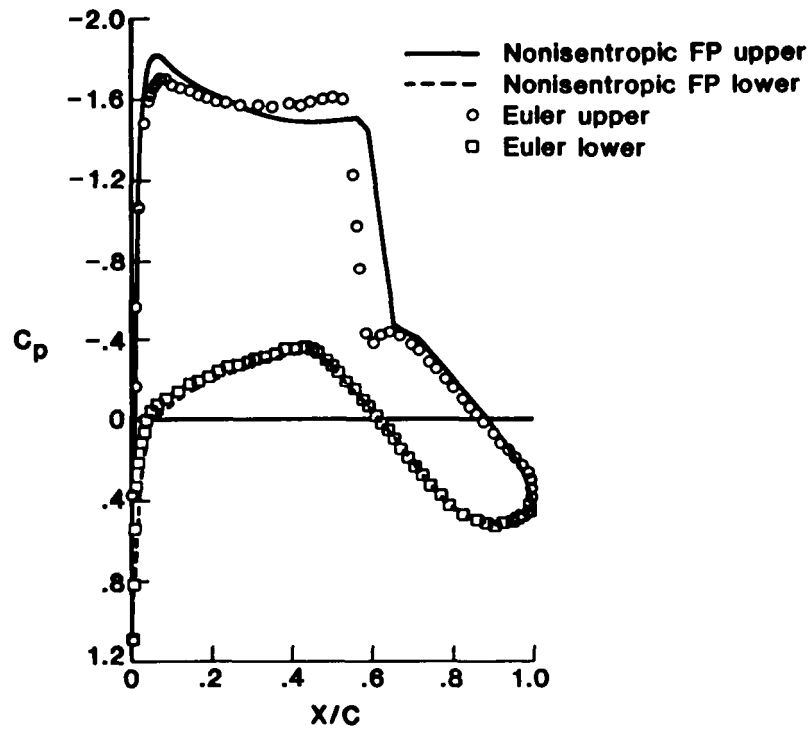
# SUMMARY

An unsteady full potential method for calculating flows with strong shock waves has been presented. The method uses approximate factorization to advance the solutions in time and a linear interpolation method to model dynamic grid motion. Calculated results were presented for the NACA 0012 and NLR 7301 airfoils.

O   PRESENTED AN UNSTEADY FULL POTENTIAL METHOD FOR FLOWS WITH STRONG SHOCKS

O   USED APPROXIMATE FACTORIZATION TO ADVANCE SOLUTIONS IN TIME

O   USED LINEAR INTERPOLATION TO MODEL DYNAMIC GRIDS

O   PRESENTED ISENTROPIC AND NONISENTROPIC CALCULATIONS FOR NACA 0012 AND NLR 7301 AIRFOILS

# CONCLUSIONS

From the results that were presented, it can be concluded that nonisentropic potential methods more accurately model Euler solutions than do isentropic methods. The primary effects of modeling shock-generated entropy are (1) to eliminate multiple flow solutions when strong shock waves are in the flow field and (2) to bring the strengths and locations of computed shock waves into better agreement with those calculated using Euler methods and those measured during experiments.

O   MODELING NONISENTROPIC EFFECTS RESULTS IN A POTENTIAL
     METHOD THAT MORE ACCURATELY MODELS EULER SOLUTIONS

O   PRIMARY EFFECTS OF MODELING SHOCK-GENERATED ENTROPY

     - MULTIPLE SOLUTIONS ELIMINATED

     - COMPUTED SHOCK WAVES IN BETTER AGREEMENT WITH
       EULER SOLUTIONS AND EXPERIMENT